

# Automatic Input Feature Relevance via Spectral Neural Networks

Lorenzo Chicchi,\* Lorenzo Buffoni, Diego Febbe, Lorenzo Giambagli, Raffaele Marino, and Duccio Fanelli  
*University of Florence, Sesto Fiorentino, Italy and  
INFN, Italy*

Working with high-dimensional data is a common practice, in the field of machine learning. Identifying relevant input features is thus crucial, so as to obtain compact dataset more prone for effective numerical handling. Further, by isolating pivotal elements that form the basis of decision making, one can contribute to elaborate on - *ex post* - models' interpretability, so far rather elusive. Here, we propose a novel method to estimate the relative importance of the input components for a Deep Neural Network. This is achieved by leveraging on a spectral re-parametrization of the optimization process. Eigenvalues associated to input nodes provide in fact a robust proxy to gauge the relevance of the supplied entry features. Unlike existing techniques, the spectral features ranking is carried out automatically, as a byproduct of the network training. The technique is successfully challenged against both synthetic and real data.

Deep Neural networks (DNNs) [1–5] are among the most popular machine learning tools, and, as such, routinely employed in a vast plethora of applications [6–9]. As for other machine learning techniques, and when employed for e.g. classification and/or regression tasks, DNNs can automatically extract valuable information from the supplied input vector. This amounts to isolate crucial components that prove decisive in implementing unmanned decision making strategies. In many cases, however, input data are naturally embedded in high dimensional spaces. This curse of dimensionality, quoting with lexical abusing from a renowned motto [10], makes it in general difficult to selectively single out, from the sea of underlying components, the subset of attributes deemed essential. Despite this degree of inherent complexity, it is of the utmost relevance to identify key input features that could be instrumental in (i) devising apt solutions for data compression and compactification; (ii) providing critical insights into the processes that led to the produced output response.

A first solution is to operate an a priori features' selection, with the aim to isolate beforehand a limited subset of supposedly relevant input elements that should undergo subsequent scrutiny [11]. This certainly yields machine learning models with a reduced dimensional load. Prior trimming criteria could however resolve in the removal of essential information, erroneously targeted as fruitless by the upstream selection.

Other methods have been proposed for post-hoc interpretability, that is, to shed light on the pathways that form the basis of decision of a trained model [12–17]. Worth mention is the so called Layer-Wise Relevance Propagation method [15, 16] which implements a back-propagation, from the output to the input space, to reach the relevant features that populate the entry layer. The method has been successfully challenged against distinct application realms [18, 19]. However, like many other approaches belonging to the same class, the latter is an

input-dependent framework and requires a certain number of operations to be carried out after training, for each examined input, so as to assess the relevance of the features for that particular supplied item.

Here, we put forward a different method with complementary objectives. The aim is to define a strategy to quantify the relative importance of different input feature, for a dataset *taken as a whole*, and for a general feedforward neural network. Unlike the aforementioned methods, the proposed metric is not input dependent. At variance, it bears universality traits, by providing a global insight on how the model oversees the input space, upon learning. Moreover, unlike standard techniques for input feature selection, the analysis is not conducted a priori on the data to be eventually scanned. The ranking of the features is indeed carried out automatically, as a byproduct of the training stage. This is achieved by establishing an ideal bridge, justified on first principles, between a pool of trainable parameters – to be optimized for task resolution – and the level of inherent relevance, as associated to different components of the input vector. At the end of the training, by accessing the values assigned to the aimed parameters, will therefore yield an automatic and self-consistent ranking of the individual input features.

To this end, we will make use of a recently introduced scheme for handling the optimization of feedforward networks, known as *spectral parametrization* [20–26]. The mathematical foundation of the spectral methodology lies within the theory of networks. From this angle, feedforward neural networks can be pictured via a dedicated spectral decomposition that materializes, in direct space, in a collection of adjacency matrices for the linear mapping of the signal across adjacent layers.

Let us begin by reviewing the basic of the spectral method [20]. We denote with  $l - 1$  and  $l$  two consecutive layers of a feedforward neural network. Assume the layers to be respectively composed by  $N$  and  $M$  nodes. The vector  $\mathbf{x}^{l-1} = (x_1^{l-1}, \dots, x_N^{l-1})$  (resp.  $\mathbf{x}^l = (x_1^l, \dots, x_M^l)$ ) stores information on the activity of the nodes belonging to layer  $l - 1$  (resp.  $l$ ). The

---

\* lorenzo.chicchi@unifi.it

linear transfer between the two adjacent layers is operated by a rectangular  $M \times N$  matrix  $W$ , whose elements read  $w_{ji}$ . Hence,  $\mathbf{x}^l = f(W\mathbf{x}^{l-1})$ , where  $f$  is a non-linear filter. Under the spectral paradigm, the above operation can be recast in an equivalent form that assumes dealing with the bipartite direct network made of the  $N + M$  nodes involved in the transfer. The state vector at the departure layer can be written as  $\mathbf{z}^{l-1} = \mathbf{x}^{l-1} = (x_1^{l-1}, x_2^{l-1}, \dots, x_N^{l-1}, 0, 0, \dots, 0)$  where we made explicit that the non trivial activity is solely localized on the nodes of the first layer. Then,  $\mathbf{z}^l = f(A\mathbf{z}^{l-1})$ , where the last  $M$  elements of vector  $\mathbf{z}^l$  refer to the activity on the destination layer;  $A$  is a  $(M + N) \times (M + N)$  matrix with a  $M \times N$  sub-diagonal block that coincides matrix  $W$ , as depicted in the annexed Appendix A. It should be noted that possible diagonal entries of matrix  $A$  do not reflect on the produced activity on layer  $l$ . One can invoke therefore a spectral decomposition of the square transfer matrix, as  $A = \Phi\Lambda\Phi^{-1}$  where (i)  $\Phi$ , the matrix of the eigenvectors, is lower-block triangular with ones on the diagonal, (ii)  $\Lambda$  identifies the diagonal matrix formed with the eigenvalues  $(\lambda_i, i = 1, \dots, N + M)$  of  $A$ . Given the specific form of matrix  $\Phi$ , it can be shown [21, 24] that  $\Phi^{-1} = 2\mathbb{I} - \Phi$ . In practical terms, the elements of  $A$ , namely those involved in the self-consistent definition of the relevant transfer matrix  $W$ , can be written as a function of the eigenvalues  $\lambda_i$  and the non trivial entries  $\psi_{ji}$  of the eigenvector matrix  $\Phi$ . An explicit calculation can be performed that yields  $w_{i \rightarrow j} = w_{ji} = (\lambda_i - \lambda_j)\psi_{ji}$ , where  $i = 1, \dots, N$  refer to nodes located on layer  $l-1$  and  $j = 1, \dots, M$  to those assigned to layer  $l$ . Further technical details are provided in Appendix A. A direct correspondence can be hence drawn between individual eigenvalues and nodes within the sampled collection. Training a feed-forward network under the spectral standpoint amounts to minimize the loss (a suitable metric that gauges the distance between produced and expected output at the exit layer) with respect to the eigenvalues and eigenvectors. In light of the existing correspondence, the magnitude of the optimized eigenvalues can be used as a reliable marker of the nodes' relevance [27], an observation that can be exploited for proposing an effective (input) feature detection algorithm, as we shall set to demonstrate in the following. To this end, we chose to operate under the simplifying assumption  $\lambda_j = 0$  (i.e. by forcing to zero the eigenvalues associated to destination nodes) yielding:

$$w_{ji} = \lambda_i \psi_{ji}. \quad (1)$$

The spectral writing of inter-nodes weights  $w_{ji}$  introduced a multiplicative factor, the eigenvalue  $\lambda_i$ , shared by all links emanating from the departure node  $i$ . The larger the magnitude of the optimized  $\lambda_i$  the more relevant the nodes for the processing of the information across the network. Specifically, we will convincingly conclude on the ability of the eigenvalues associated to the starting layer  $l = 1$  to automatically discriminate between irrelevant and relevant input features. Further, we will show that eigenvalues (multiplied by the norm of the corresponding

eigenvector entry) can be exploited to rank the relative importance of the features otherwise deemed as irrelevant. The method will be tested against classification problems constructed from mock and real datasets. For all examined cases, a penalty is added to the loss function as in the spirit of [25]. This is a  $L_2$  regularization of  $\lambda_i$  which forces eigenvalues associated with irrelevant components to be set to zero (and not just left unaltered to their initial values, possibly drowned in the sea of their relevant homologues). It is worth stressing that in principle it is enough to have just the first layer parameterized as spectral for this analysis to apply. For further details on the training procedure refers to Appendix B.

**Independent Gaussian distributions dataset** The first dataset is structured with 2 target classes and input vectors with 20 independent features. Each data component is sampled from a Gaussian distribution. While some components are drawn from distributions which are set to be identical across classes, others display only partial overlap. Components with identical distributions offer no discriminatory information. As such, they prove ineffective for classification purposes. Conversely, non trivial components are pivotal, the smaller the overlap the larger their relevance in promoting the sought discrimination.

A spectral feedforward neural network, parametrized as stipulated by Eq. (1), has been trained with the aim of assigning input from the above dataset to the correct class of origin. The employed network consists of three hidden layers with, respectively, 100, 100, and 50 neurons. In addition, the network accommodates for an input layer of size 20 and an output layer of size 2. At the end of the training, we analyzed the 20 eigenvalues, associated with the input layer as in the spirit of the above discussion (with an abuse of language we will from here call eigenvalues the rescaled version of this latter which incorporate the norm of the eigenvectors, as stipulated in Appendix A). As shown in panel (a) of Fig. 1, eigenvalues entangled with irrelevant features are all zero, while eigenvalues which can be traced back to relevant input components are non-zero. Hence, the eigenvalues interfused with the input layer can efficiently tag features identified as relevant by the network itself to solve the assigned task. The magnitude of non-zero eigenvalues, i.e., those associated with relevant components, is found to correlate with a direct measure of the relative distance between the distributions from which individual components are drawn (see panel (b) of Fig. 1). Since the distributions differ only in their mean value, we quantify the above distance as the absolute value of the difference between the two means.

**Correlated Gaussian distributions dataset** Unlike the dataset just analyzed, real datasets often exhibit correlations between input vector components, and crucial task-solving information are frequently concealed within those correlations. With this motivation in mind, we tested the proposed spectral feature detection method on a different dataset that contains pairwise correlations

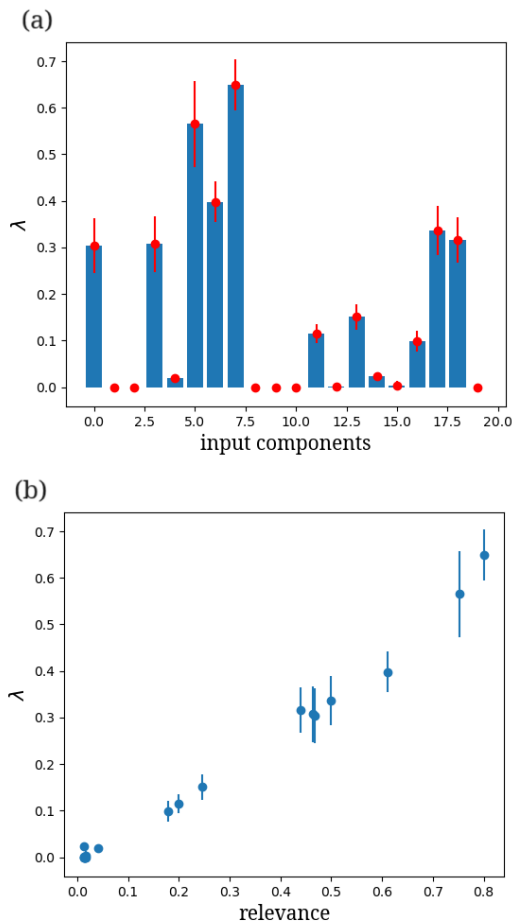


FIG. 1. Panel (a) displays the 20 post-training eigenvalues associated to the input layer, for the *simple Gaussian dataset*. The red dots and the red bars correspond to the average values and the standard deviations of the results obtained by repeating the experiments for 10 independent realizations. In panel (b) the same post-training eigenvalues are reported against a relevance parameter that gauges the distance between the distributions (respectively blue and red, in Fig. 5) from which the components are eventually drawn. The distance is defined as the absolute value of the difference between the two means.

between input vector components. The dataset is still organized into two distinct classes that are to be eventually identified. Input vectors are now made of 10 components. The first 8 components are defined as follows:

$$\begin{aligned}
 x_{2n} &\sim \mathcal{N}(0, 1) \\
 x_{2n+1} &= x_{2n} && \text{if } c(\vec{x}) = 0 \\
 x_{2n+1} &= \begin{cases} x_{2n} & \text{with prob. } 1-p \\ -x_{2n} & \text{with prob. } p \end{cases} && \text{if } c(\vec{x}) = 1
 \end{aligned} \tag{2}$$

where  $c(\vec{x})$  is the target class of the input and  $n \in \{0, 1, 2, 3\}$ . The last two components are independently drawn from two identical normal distributions  $\mathcal{N}(1, 0)$

regardless of the class of belonging:

$$x_8, x_9 \sim \mathcal{N}(0, 1). \tag{3}$$

As a first noticeable observation, we remark that it is not possible to separate the two datasets by solely relying on independent observations of the respective vector components. Indeed, crucial information are reflected in how pairs of components are mutually correlated.

To better understand the relationship between the different components, let us focus on the first two entries of the input vectors,  $x_0$  and  $x_1$ . For data belonging to class 0 (as we label the first of the two)  $x_0 = x_1$ , that is, the first two components are perfectly correlated. Conversely, the two components of data belonging to the other class (denoted by 1) are equal with probability  $1-p$  and have opposite sign with probability  $p$ . If  $p = 0$ , the first two components are equal for both classes. No information about the class to which the supplied data belong can be thus extracted by comparing the two above components. The second component is indeed a mere copy of the first and therefore irrelevant for classification purposes. Conversely, if  $p = 1$ , the first and second components from class 1 data are in perfect anti-correlation, while data from class 0 are still matched and thus fully correlated. Hence, in the latter case, it is possible to completely separate the two classes by solely comparing  $x_0$  and  $x_1$ . Parameter  $p$  quantifies therefore the degree of sensible information which can be pulled out from a direct comparison of the two aforementioned components. Finally, the last two components are not correlated to the others and identically distributed for both classes, hence devoid of information. We hence assign a parameter  $p = 0$  to these two components to explicitly state their manifest irrelevance.

The architecture of the employed neural network, parametrized via its spectral modality, is identical to that put forward for the analysis of the uncorrelated dataset (except for the first layer that in this case receives just 10 entries). In panel (a) of Fig. 2, the post-training eigenvalues referred to the input layer are shown. Firstly, we notice that pairs are correctly spotted out, as they are assigned the very same eigenvalue entry. Moreover, eigenvalues associated with irrelevant components are tuned zero for this dataset as well, an observation that testifies again on the ability of the spectral network to discriminate between irrelevant and relevant features. Lastly, the magnitude of the recorded eigenvalues scales proportionally to the control parameter  $p$ , which quantifies the relevance of the selected pair for classification purposes (panel (b), Fig. 2). In conclusion, and also for this second, more complex dataset, the optimized eigenvalues referred to the first layer are a good proxy of the importance of the associated components.

**The MNIST dataset** As a final test, we applied the spectral features detection method to a reduced version of the well-known MNIST dataset [28]. This latter consists of  $28 \times 28$  images depicting handwritten digits, ranging from 0 to 9, to be eventually classified. In our experi-

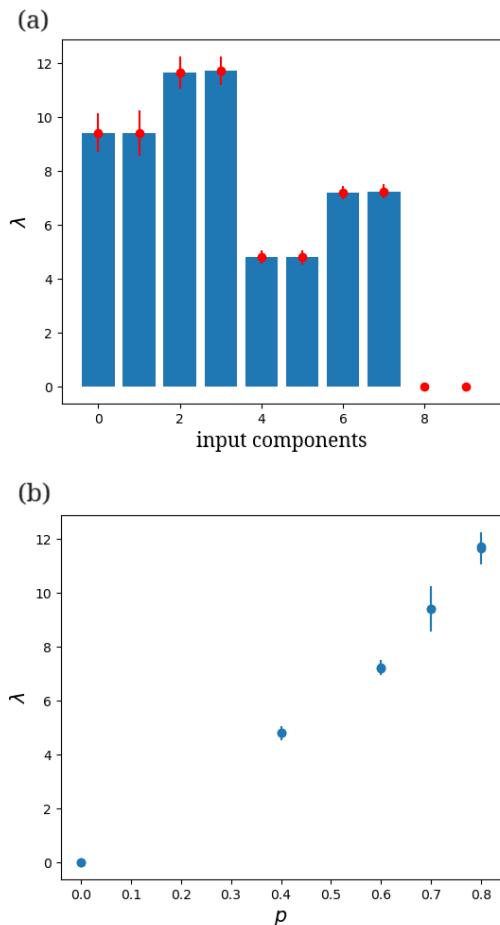


FIG. 2. Panel (a) reports the ten post-training eigenvalues (referred to the input layer) for the *correlated Gaussian dataset*. Red dots and red bars quantifies the recorded average values and the associated standard deviations, as obtained by averaging over 10 independent realizations. In panel (b) the same post-training eigenvalues are plotted against the parameter  $p$ , as defined in the main text

ments, and to deliver a clear message, we just focused on the subset of images “zeroes” and “ones”. Despite the simplicity of the adopted framework, it is interesting to test the method against a real dataset, where the measure of the relevance of the components is not a priori given. The input vectors of the MNIST dataset has a dimension of 784, and each component of the vectors represents the intensity of a specific pixel in the corresponding image.

In this context, asking which component is relevant amounts to asking which pixel (or collection of pixels) discloses the information that is used by the trained network to make decision.

Once again, we trained a spectral feedforward neural network by adjusting the trainable spectral parameters. The hidden structure of the network is identical to that employed for the above applications. Clearly, the input layer is now made of 784 elements, the size of the sup-

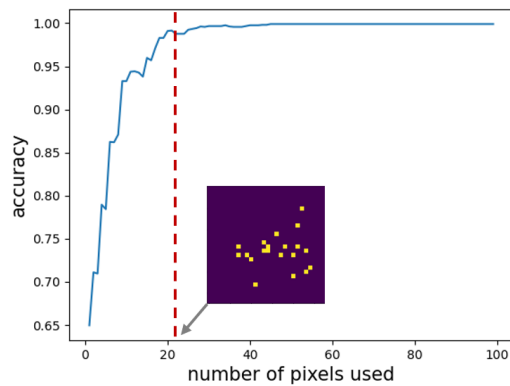


FIG. 3. The blue line refers to the accuracy of the model as the number of pixels taken as input grows. The order in which the pixels are inserted follows the absolute value (magnitude) of their corresponding post-training eigenvalues. In the inset, the input space is represented, with the twenty most important pixels highlighted.

plied items. The exit layer is still composed of just two nodes, one associated to the images that display a zero and the other pointing to the ones. As expected, the trained model performs very well in terms of estimated classification accuracy (largest than 99 %).

The distribution of the post training eigenvalues associated to the input layer shows a clear peak at zero, signifying that many eigenvalues have been suppressed, thus targeted as ineffective, during training stages. Just a few eigenvalues take non-zero values (see Fig. 7 in Appendix C). This conclusion can be rephrased by stating that many pixels are unnecessary for task resolution.

The accuracy of the trained network gets modulated as a function of the number of input pixels included in the analysis, see Fig. 3. In this latter Figure, we progressively include more and more pixels ranked from the most to the least important, as according to the spectral (i.e. eigenvalues magnitude) metric. Remarkably the computed accuracy raises rapidly, with a sharp, almost abrupt approach to asymptotic convergence, a trend that cannot be reproduced by employing any other set of identical cardinality of randomly selected pixels. In particular, by arbitrarily fixing the number of pixels to be included (in descending order of importance) to 20, one obtains a final accuracy which is competitively close to that recorded when the full load of pixels is provided at the input layer. These 20 pixels, ranked as most important and sufficient for the correct functioning of the trained classification algorithm, can be located back on the 2D grid that defines the images support (inset in Fig. 3).

To figure out how the network exploits the subset of selected pixels for handling the classification task, we can overlay the mask containing only the relevant pixels (the binarized picture displayed as inset in Fig. 3) on individual input (images) data. A few examples of what one gets following this procedure are reported in Fig. (4).



The part of  $A$  responsible of the information transfer from the departure layer  $l - 1$  to the destination layer  $l$  is the the bottom-left block  $W$ . The relation between the elements of  $W$  and the spectral parameters (i.e., the non-zero elements of the matrix  $\Lambda$  and the elements of the  $\Psi$  block of the eigenvector matrix) can be analytically computed yielding

$$w_{i \rightarrow j} = w_{ji} = (\lambda_i - \lambda_j)\psi_{ji}. \quad (\text{A4})$$

The weights  $w_{ji}$ , (associated in the standard formulation to the links of the feedforward network to be trained) are now functions of the spectral attributes of matrix  $A$ . Following this alternative parametrization, the target of the optimization are the components and the eigenvectors and the corresponding eigenvalues. From optimized eigenvectors and eigenvalues one can compute the weight of the transfer matrix in direct space via equation (A4). The markers used for discriminating relevant features are the eigenvalues of  $A$  rescaled by a quantity that accounts for the norm of the associated eigenvectors, in accordance with what was done in [25, 26]. In formulae,  $\tilde{\lambda}_i = \lambda_i \left( \sum_j \phi_{ji} \right)^{1/2}$ . All along the paper we drop the tilde and refer to  $\tilde{\lambda}_i$  as to the  $i$ -th eigenvalue of matrix  $A$ .

## Appendix B: Training procedure

In this Appendix, we provide detailed information on the training procedures. The optimization process for all three datasets discussed in the main text was conducted using the Adam optimizer [29]. The learning rates were set to 0.01 for the first two datasets and 0.0001 for MNIST. Sparse Categorical Crossentropy was employed as the loss function for all three tasks. The number of epochs was set to 1000 for the Gaussian dataset, 500 for the correlated Gaussian dataset, and 5000 for MNIST. The results presented in the manuscript demonstrated robustness to variations in these hyperparameters. Therefore, the hyperparameters were manually optimized from a restricted set of possible candidates by assessing the model's performance on a validation set (10 % of the training set).

## Appendix C: Datasets

In this Appendix, we clarify the structure of the datasets that we have generated to validate the method. Fig. 5 shows the distributions of the input components for the dependent Gaussian dataset. In the first two panels of Fig. 6 The distributions of the values of the fourth and fifth components of the input vectors in the *correlated Gaussian dataset* are reported, while in the bottom panel, the same components are plotted against each other.

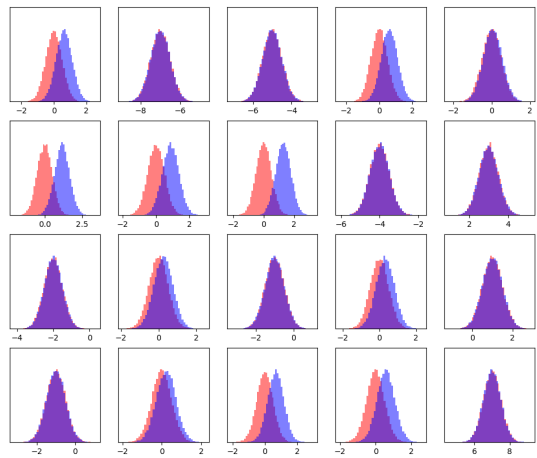


FIG. 5. Distribution of the values of the 20 components of the input vectors in the *independent Gaussians dataset*. The distributions for the data belonging to the first (resp. second) class are represented in red (resp. blue). For some components, the two classes are indistinguishable, while in some other cases the two distributions are only partially overlapping.

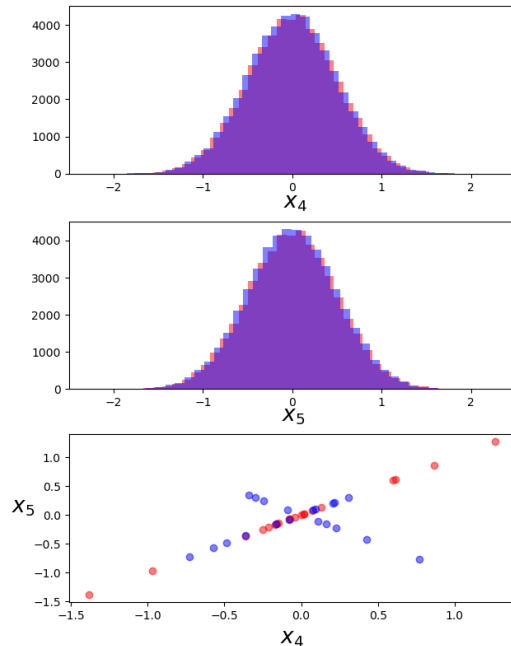


FIG. 6. The distributions of the values of the fourth and fifth components of the input vectors in the *correlated Gaussian dataset* are shown in the first two panels. In the bottom panel, the fifth component is plotted against the corresponding fourth component for some input vectors of the same dataset. Individually, both components contain no information on the vector classes. However, by observing their correlations, a certain degree of asymmetry can be appreciated for data belonging to different classes. By analyzing the two components simultaneously one can therefore acquire useful information to solve the classification task.

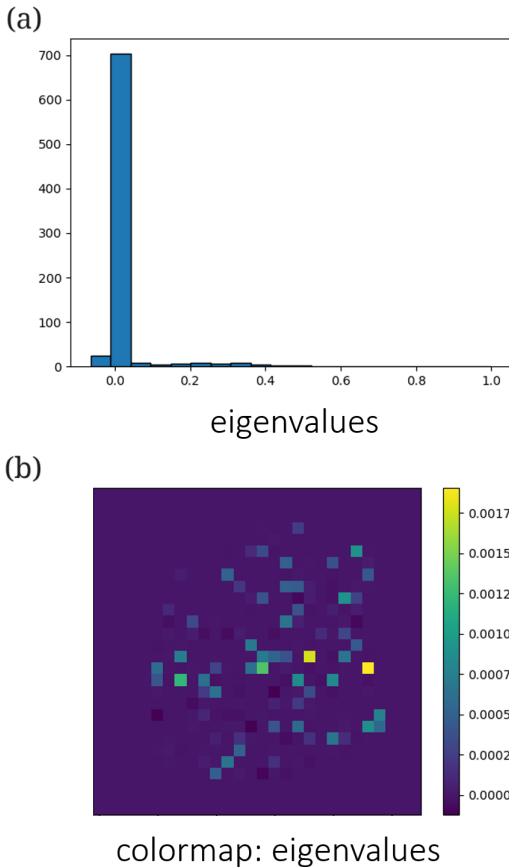


FIG. 7. In panel (a) the distribution of the first 784 post-training eigenvalues (normalized to their maximum) for the MNIST dataset is reported. Panel (b) shows the input space for the same dataset, where each component (i.e., pixel) is colored according to its relative post-training eigenvalue.

#### Appendix D: Post-training eigenvalues distribution for the MNIST dataset

We report here the distribution of the eigenvalues obtained at the end of the training for the MNIST dataset. Specifically, the distribution is shown in panel (a) of Fig. 7 and exhibits a peak at zero, as already mentioned in the main body of the paper. The presence of this peak demonstrates the irrelevance of a large fraction of the input features. The presence of this peak demonstrates the irrelevance of a large fraction of the input features. The presence of this peak demonstrates the irrelevance of a large fraction of the input features. The presence of this peak demonstrates the irrelevance of a large fraction of the input features.

- 
- [1] L. Deng, D. Yu, *et al.*, Deep learning: methods and applications, Foundations and trends<sup>®</sup> in signal processing **7**, 197 (2014).
  - [2] I. Goodfellow, Y. Bengio, and A. Courville, *Deep learning* (MIT press, 2016).
  - [3] Y. LeCun, Y. Bengio, and G. Hinton, Deep learning, nature **521**, 436 (2015).
  - [4] S. J. Prince, *Understanding Deep Learning* (MIT press, 2023).
  - [5] G. Carleo, I. Cirac, K. Cranmer, L. Daudet, M. Schuld, N. Tishby, L. Vogt-Maranto, and L. Zdeborová, Machine learning and the physical sciences, Reviews of Modern Physics **91**, 045002 (2019).
  - [6] S. Chmiela, A. Tkatchenko, H. E. Sauceda, I. Poltavsky, K. T. Schütt, and K.-R. Müller, Machine learning of accurate energy-conserving molecular force fields, Science advances **3**, e1603015 (2017).
  - [7] L. Chicchi, L. Bindi, D. Fanelli, and S. Tommasini, Frontiers of thermobarometry: Gaia, a novel deep learning-based tool for volcano plumbing systems, Earth and Planetary Science Letters **620**, 118352 (2023).
  - [8] T. Biancalani, G. Scalia, L. Buffoni, R. Avasthi, Z. Lu, A. Sanger, N. Tokcan, C. R. Vanderburg, Å. Segerstolpe, M. Zhang, *et al.*, Deep learning and alignment of spatially resolved single-cell transcriptomes with tangram, Nature methods **18**, 1352 (2021).
  - [9] P. Baldi, P. Sadowski, and D. Whiteson, Searching for exotic particles in high-energy physics with deep learning, Nature communications **5**, 4308 (2014).
  - [10] R. Bellman, Dynamic programming, science **153**, 34 (1966).
  - [11] I. Guyon and A. Elisseeff, An introduction to variable and feature selection, Journal of machine learning research **3**, 1157 (2003).
  - [12] W. R. Swartout and J. D. Moore, Explanation in second generation expert systems, in *Second generation expert systems* (Springer, 1993) pp. 543–585.
  - [13] G. Montavon, W. Samek, and K.-R. Müller, Methods for interpreting and understanding deep neural networks, Digital signal processing **73**, 1 (2018).
  - [14] D. Baehrens, T. Schroeter, S. Harmeling, M. Kawanabe, K. Hansen, and K.-R. Müller, How to explain individual classification decisions, The Journal of Machine Learning

- Research **11**, 1803 (2010).
- [15] G. Montavon, A. Binder, S. Lapuschkin, W. Samek, and K.-R. Müller, Layer-wise relevance propagation: an overview, *Explainable AI: interpreting, explaining and visualizing deep learning*, 193 (2019).
- [16] S. Bach, A. Binder, G. Montavon, F. Klauschen, K.-R. Müller, and W. Samek, On pixel-wise explanations for non-linear classifier decisions by layer-wise relevance propagation, *PloS one* **10**, e0130140 (2015).
- [17] S. Bazen and X. Joutard, The taylor decomposition: A unified generalization of the oxaca method to nonlinear models, (2013).
- [18] M. Böhle, F. Eitel, M. Weygandt, and K. Ritter, Layer-wise relevance propagation for explaining deep neural network decisions in mri-based alzheimer’s disease classification, *Frontiers in aging neuroscience* **11**, 194 (2019).
- [19] Y. Yang, V. Tresp, M. Wunderle, and P. A. Fasching, Explaining therapy predictions with layer-wise relevance propagation in neural networks, in *2018 IEEE International Conference on Healthcare Informatics (ICHI)* (IEEE, 2018) pp. 152–162.
- [20] L. Giambagli, L. Buffoni, T. Carletti, W. Nocentini, and D. Fanelli, Machine learning in spectral domain, *Nature communications* **12**, 1330 (2021).
- [21] L. Chicchi, L. Giambagli, L. Buffoni, T. Carletti, M. Ciavarella, and D. Fanelli, Training of sparse and dense deep neural networks: Fewer parameters, same performance, *Physical Review E* **104**, 054312 (2021).
- [22] L. Chicchi, D. Fanelli, L. Giambagli, L. Buffoni, and T. Carletti, Recurrent spectral network (rsn): Shaping a discrete map to reach automated classification, *Chaos, Solitons & Fractals* **168**, 113128 (2023).
- [23] L. Chicchi, L. Giambagli, L. Buffoni, R. Marino, and D. Fanelli, Complex recurrent spectral network, arXiv preprint arXiv:2312.07296 (2023).
- [24] L. Buffoni, E. Civitelli, L. Giambagli, L. Chicchi, and D. Fanelli, Spectral pruning of fully connected layers, *Scientific Reports* **12**, 11201 (2022).
- [25] L. Giambagli, L. Buffoni, L. Chicchi, and D. Fanelli, How a student becomes a teacher: learning and forgetting through spectral methods, *Advances in Neural Information Processing Systems* **36** (2024).
- [26] L. Giambagli, L. Buffoni, L. Chicchi, and D. Fanelli, How a student becomes a teacher: learning and forgetting through spectral methods, *J. Stat. Mech.: Theory Exp.* **2024** (3).
- [27] The usage of the eigenvalues as an indirect measure of the nodes relevance has been explored in [21, 24, 25]. An effective trimming strategy was in particular proposed in [24] which enables for the trained network to be significantly reduced, ex post, by cutting nodes flagged as unimportant. By leveraging on the eigenvalues and their associated magnitudes, it was possible in [25] to estimate the hidden dimension of the target objective function under analysis.
- [28] L. Deng, The mnist database of handwritten digit images for machine learning research, *IEEE Signal Processing Magazine* **29**, 141 (2012).
- [29] D. P. Kingma and J. Ba, Adam: A method for stochastic optimization, arXiv preprint arXiv:1412.6980 (2014).